*Thermochimica Acta*, 101 (1986) 245–269
Elsevier Science Publishers B.V., Amsterdam – Printed in The Netherlands



# REACTION KINETICS AT LINEARLY INCREASED TEMPERATURE. V. DTA AND UV STUDY OF THE OXIDATION OF MALONIC, TARTRONIC, GLYOXYLIC AND MONOBROMOMALONIC ACIDS BY CERIC SULPHATE IN DILUTE SULPHURIC ACID

ERHARD KOCH

*Max-Planck-Institut fuer Strahlenchemie, D-4330 Mülheim a.d. Ruhr (F.R.G.)*

(Received 14 October 1985)

## ABSTRACT

DTA and non-isothermal UV measurements of the oxidation of malonic, tartronic, glyoxylic and monobromomalonic acids by ceric sulphate in dilute aqueous sulphuric acid were evaluated using the novel one-step strategies for the determination of quantities typical of mechanism.

Due to the kinetic evaluation, experiments with malonic acid reveal the expected bimolecular reaction only in definite concentration ranges. For very small ceric ion concentrations, the large resulting reaction heats suggest that ceric ion catalyzes the oxidation of malonic acid and its oxidation products, via the corresponding organic radicals and intermediate addition of molecular oxygen. If the concentration is raised, different scenarios in a rather complex mechanism are passed, which include situations of first-order, zeroth-order, autocatalytic and consecutive character with crossing-over effects. For sufficient concentration of the cerium salt, the kinetics are influenced by repetitive oxidation of malonic acid to tartronic and glyoxylic acid by the metal salt.

This interpretation is in accordance both with results of experiments with tartronic acid and glyoxylic acid as well as with attempts to simulate the experimental signals approximately using a model of seven coupled reactions.

## INTRODUCTION

Oxidations of organic dicarbonic acids by multivalent metal salts are important processes in the Belousov–Zhabotinsky oscillating systems, which were intensively studied by Noyes and co-workers [1,2]. Thus, the reactions of ceric sulphate with malonic acid (MA) and monobromomalonic acid (BMA) were considered as constituent elements representing step No.5 in the "Oregonator mechanism", which describes the simplest model for this best-understood oscillating reaction [3,4]. This step was considered as responsible for the regeneration of bromide ion, the "trigger" substance for the appearance of the oscillations. However, this reaction is really very

0040-6031/86/$03.50 

complicated and, therefore, a subject of various further studies [5–8]. Barkin et al. [9,10] succeeded in reproducing the observed reaction kinetics at isothermal conditions by computer simulations, based on a mechanism with tartronic acid (TA) and glyoxylic acid (GLY) as transients [11].

The promising results of the non-isothermal DTA studies both with the catalyzed [4,12] and uncatalyzed [13] oscillating reactions with bromate suggested studying the attributed oxidations with ceric ion by this technique, because stoichiometric and kinetic problems may be discussed, using recent progress in the estimation of those general kinetic data which characterize the type of process, shape index and reaction type index [13–15]. Moreover, a parallel non-isothermal UV absorption study [16] should yield additional information because it can be focussed on the ceric ion. In this publication, the first examples are presented where the four elaborate strategies for the kinetic interpretation of series of thermoanalytical experiments [14,17,18] are combined, allowing a comparison of their efficiencies; i.e., discussion of:

---

Fig. 1. Evaluation of a particular DTA experiment. Computer plots (program DTAON [14,20,24,25]). (A) Smoothed original curve, and extrapolated baseline. (B) Plot of log $k$ versus $(1/T)\times 10^3$.

*Experiment*

$Ce(SO_4)_2$ + malonic acid (under argon).

*Input data*

Concentrations: 0.03; 0.02 M

Solvent: No. 29 (1 M aq. sulphuric acid).

Heating rate: 2K $min^{-1}$ (redetermination: 1.986).

*Output data*

Max. signal height: 0.332 K.

Temperatures: initial, 268.6; max., 318.1; end, 377.9 K.

Kinetic results:

| | First order | | Second order | |
|---|---|---|---|---|
| | Initial | Overall | Initial | Overall |
| Activation energy (kcal $mol^{-1}$) | 11.31 | 11.45 | 11.83 | 14.98 |
| Pre-exponential factor (log, min) | 6.95 | 6.99 | 8.95 | 11.29 |
| Specific time (min) | 9.00 | 9.02 | 8.22 | 6.44 |

Reference orders used: 2;2; halfwidth: 52.1; corr. 41.74 K; shape index: 1.09; corr. 0.762; corr. to 1:1 molar ratio: 0.895.

Reaction type index, $M$: 0.00422 (initial); 0.00331 kcal $mol^{-1}$ $K^{-1}$ (overall); correction to 1:1 molar ratio: 0.00313.

Reaction coefficient (cf. [4]): 0.809 (complex).

*Interpretation*

Orders: from halfwidth: 1.3; from shape index: 1.97. Shape index + initial $M$-index = AB type or mixed-order concurrent reactions.

Shape index + overall $M$-index = AB type or consecutive reactions.

(1) temperature/peak height plots;

(2) concentration and heating rate plots in the mechanistic diagram;

(3) heats, activation parameters and their correspondence to rate-determining steps;

(4) studies to reproduce various experimental curves from theoretical models (using the integration program METEX [17]).

## EXPERIMENTS AND EVALUATION

The reagents used were commercial charges of analytical grade. The solvent was 1 M aqueous $H_2SO_4$. The DTA experiments with 5 ml samples

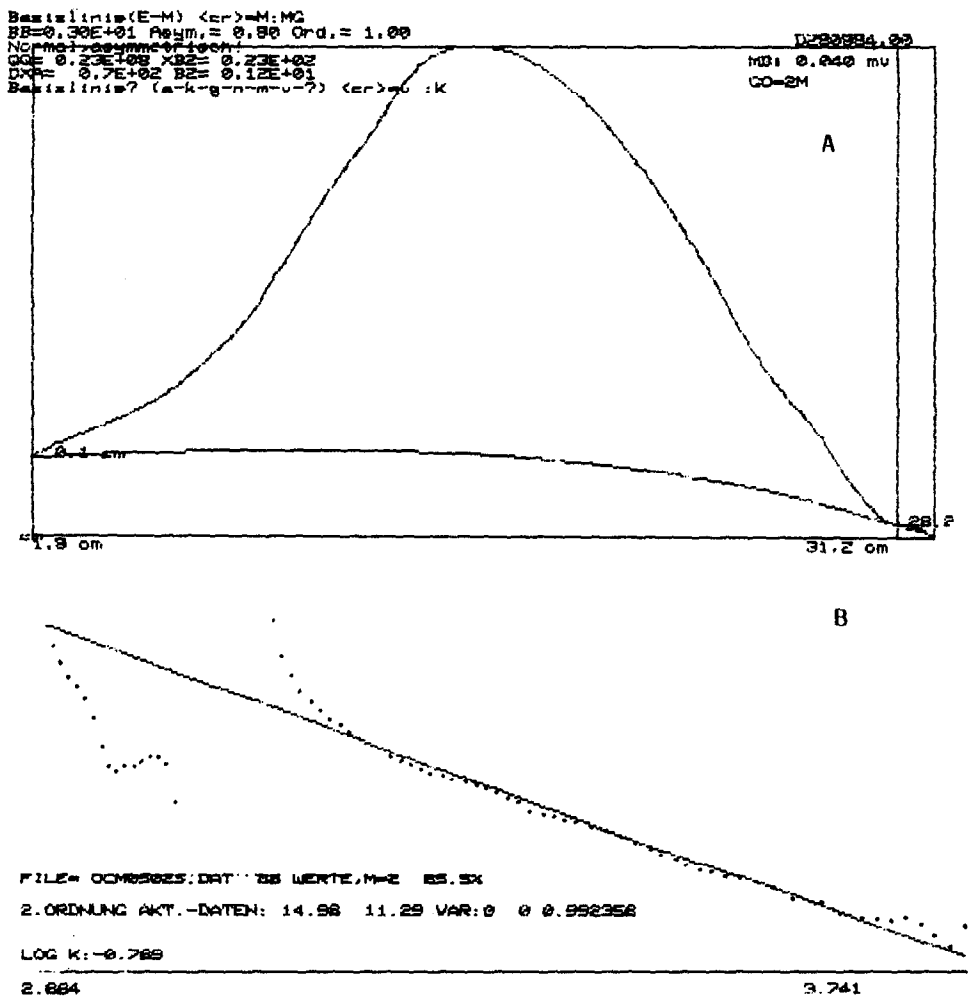

were performed in our "all-liquid" apparatus [19]. UV measurements were made, following the extinction at 317.5 nm in our double-beam spectrometer (type SEM Brückl HRS-4001C), as described in ref. 16. A constant heating rate was obtained for both apparatuses by Eurotherm temperature controllers. Special studies excepted, the access of oxygen was not excluded.

The measured kinetic curves were stored as data sets of ca. 2000 points, smoothed by a Sawitzky–Gohler algorithm and restricted to ca. 150 points which show enough detail for an accurate evaluation [15].

For the calculation of the (partially apparent) activation data and the mechanistic indices, the one-step strategy described [14,20,21] was applied both for the total signals as well as for some separable single peaks (programs DTA, DTAON). Figure 1A indicates the computer printout with the smoothed DTA curve, baseline, input and output data, and the results of the kinetic interpretation (program DTAON) for an individual experiment. Figure 1B shows the Arrhenius plot for an assumed bimolecular process (program ARR [14]).

The experimental series are, together with the reaction enthalpies, presented in Table 1; in all cases, either the starting concentration of one reactant or the heating rate was varied from experiment to experiment. Because of the relatively small concentration gap between transparency and total absorption in the sample, the DTA studies cover a considerably larger range of concentration than the (more sensitive) UV technique.

The last two columns of Table 1 show the approximate enthalpies of such experiments in ranges where there was no considerable enthalpy variation, together with the corresponding average concentration or heating rate. Figure 2 shows an experimental series, subsequent to subtraction of the extrapolated baseline (initially linear, later adapted exponential function) and based on a common temperature axis. Splitting, merging, appearance and disappearance of peaks are distinctly summarized by such a representation, showing the dependence on an initial concentration or on the heating rate.

In Fig. 3, experiments with different substances, but equal or similar starting concentrations are also compared; typical DTA curves and the extinction change curves for the four title compounds are listed, revealing that malonic acid in general gives one (often distorted) peak, whereas the other compounds render several, often less distinct signals.

As a general strategy for the interpretation of the series experiments, we used pattern recognition in various types of diagrams, and comparison with computer-generated theoretical model series. Figure 4 gives examples of plots initial temperature $T_0$ vs. relative signal height, referred to the initial concentration of the varied reactant as parameter, both for DTA and UV series. Such three-dimensional representations of the results for a series in a plane seem illustrative, but are not an appropriate form to be read by the computer, because the parameter "concentration" is not directly revealed.

TABLE 1

Experimental series and reaction enthalpies

| Series [a] | Acid | Expts. | Method | $m$ (K $min^{-1}$) | Concentrations ($10^3$ M) | | Heat (kJ $mol^{-1}$) per mole of varied reactant [b] | | |
|---|---|---|---|---|---|---|---|---|---|
| | | | | | $Ce(SO_4)_2$ | Acid | Range [c] | Typical experiment in range of const. $\Delta H$ | |
| | | | | | | | | Heat [c] | Conc. or heating rate |
| 1 | MA | 18 | DTA | 1.50 | 2–27 | 25 | 42–1800 | 410 | 0.012 |
| 1i | | 18 | | 1.55 | 25 | 2.5–375 | 140–280 | 215 | 0.03 |
| 1u | | 11 | UV | 1.50 | 0.05–0.5 | 3.75 | (103–191) | (180) | 0.1 |
| 1iu | | 8 | | 1.50 | 0.251 | 3–3.8 | (12–30.2) | (30) | 0.003 |
| 1h | | 7 | DTA | 0.25–4 | 25 | 25 | 75–443 | 190 | $m = 1.4$ |
| 1hu | | 16 | UV | 0.36–4.6 | 0.25 | 1.55 | (3.3–97) | (38) | $m = 1$ |
| 2 | TA | 8 | DTA | 1.2 | 5–120 | 0.1 | 44–100 | 46 | 0.08 |
| 2$\alpha$ | | 8 | | 0.75 | 5–120 | 0.1 | 33–100 | 31 | 0.09 |
| 2i | | 10 | | ~1 | 15 | 5–15 | 14–47 | 25 | 0.01 |
| | | | | ~1 | 15 | 25–200 | 3.3–4.6 | 12.8 | 0.15 |
| 2i$\beta$ | | 8 | | 1.4 | 15 | 25–200 | 3.3–4.6 | ~ 2.1 | 0.03 |
| 2u | | 10 | UV | 1.47 | 0.15–0.5 | 2.44 | (14–115) | (74) | 0.0004 |
| 2u | | 7 | | 1.2 | 0.15–0.45 | 2.44 | (8–24) | (24) | 0.0004 |
| 2hu | | 7 | | 0.44–6.9 | 0.24 | 1.5 | (14–197) | (197) | $m = 0.45$ |
| 3 | GLY | 12 | DTA | 1.35 | 0.75–40 | 15 | 42–2200 | 78 | 0.01 |
| 3$\alpha$ | | 12 | | 1.2 | 4–40 | 15 | 19–52 | 20 | 0.01 |
| 3$\beta$ | | 12 | | 1.4 | 0.75–40 | 15 | 1.7–930 | 58 | 0.007 |
| 3u | | 8 | UV | 1.52 | 0.1–0.5 | 2.44 | (10–670) | (55) | 0.00024 |
| 3iu | | 8 | | 1.55 | 0.25 | 0.25–5 | (5–164) | (10) | 0.00018 |
| 3hu | | 11 | | 0.67–6.7 | 0.25 | 1.5 | (15–90) | (83) | $m = 1.6$ |
| 4 | BMA | 8 | DTA | 1.5 | 2.5–10 | 37.5 | 25–267 | ~ 370 | 0.006 |

[a] No index i, normal DTA series; $Ce^{4+}$ is varied. i, inverse series; acid is varied. u, UV series. h, heating rate series. $\alpha$, $\beta$, only the $\alpha$ ($\beta$) peak is evaluated. (Example: 2i$\beta$ = DTA series of system $Ce(SO_4)_2$ + TA where $[TA]_0$ is varied; the second peak is evaluated.)

[b] Heating rate series: reference to $[Ce(SO_4)_2]_0$.

[c] Increase of extinction at 317 nm, referred to concentration of varied reactant (or of $[Ce^{4+}]_0$ in heating rate series).

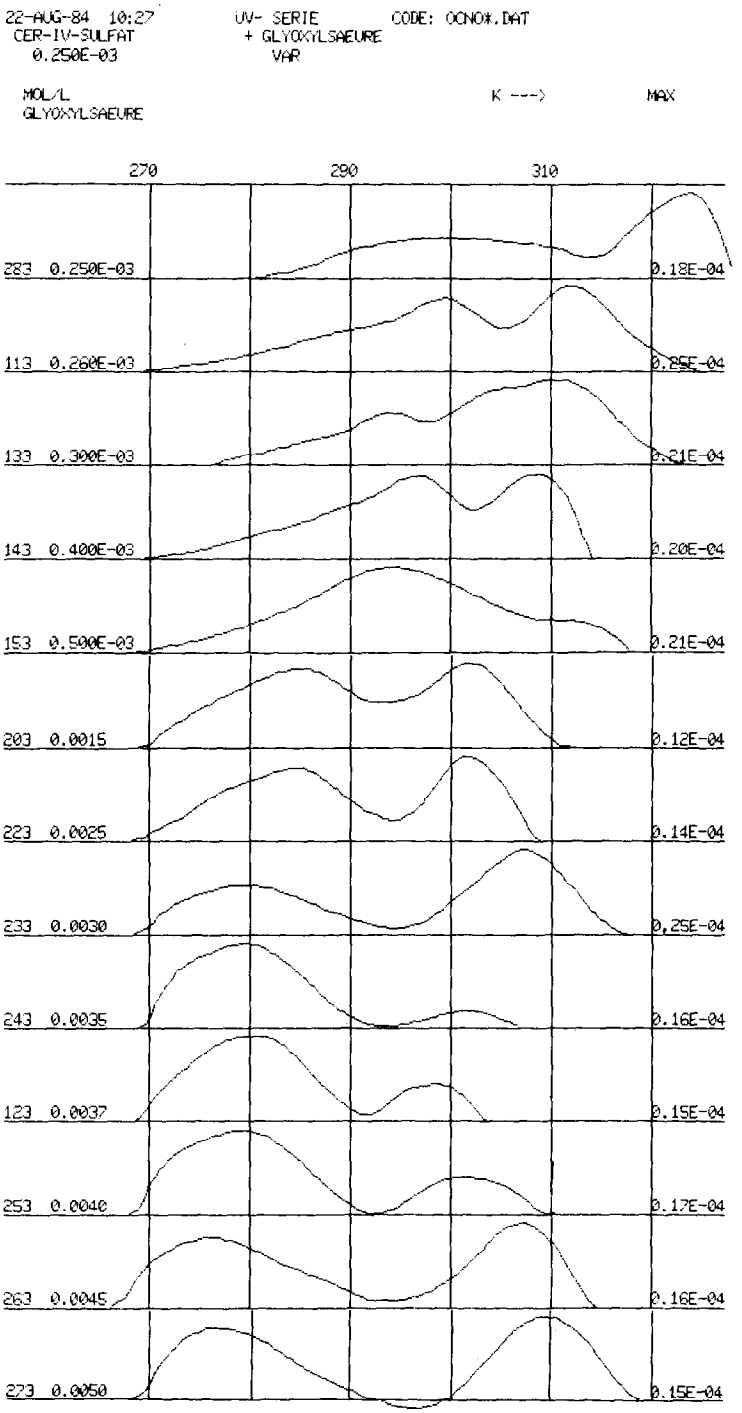


Fig. 2. Non-isothermal UV signals of a concentration series (ceric sulphate + glyoxylic acid.) Computer form. Ordinate: rate of extinction change. Heating rate: 1.5 K $min^{-1}$. Temperature range: 270–328 K. First column: experiment No., concentration of GLY. Last column: maximum signal height (here, maximum reaction rate $\times 10^{-4}$).

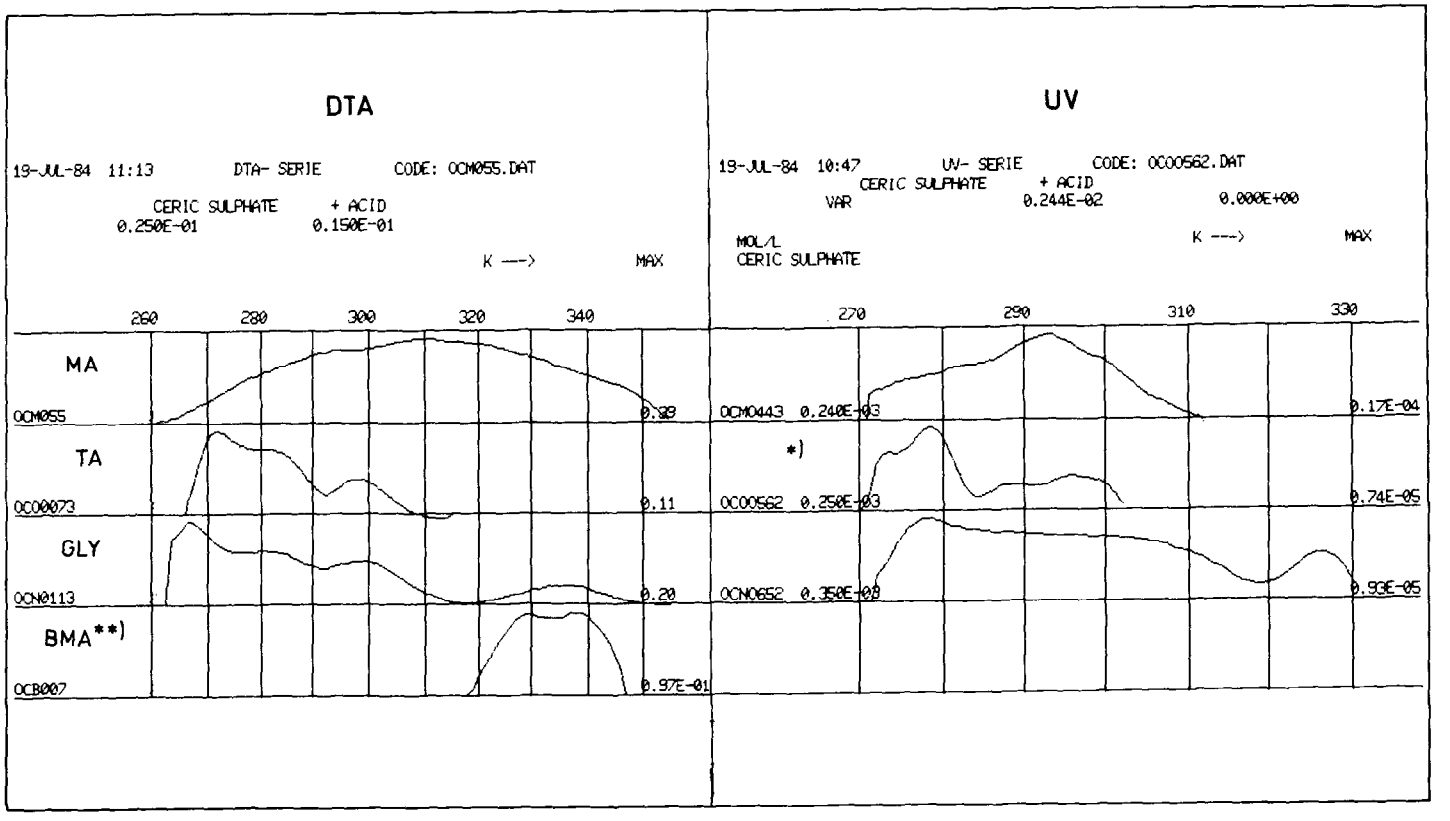


Fig. 3. Comparison of DTA and UV signals of the reactions of the four acids. Computer forms: (*) concentrations of both components are equal (0.00025 M); (**) monobromomalonic acid.

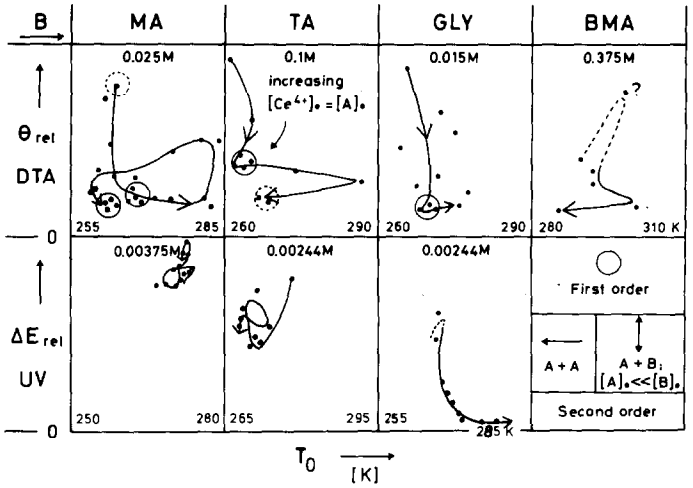


Fig. 4. Temperature/signal height plots for the "normal" series (ceric sulphate varied). Programs KOBIB, GRAF [14,17]. Abscissa: initial temperature $T_0$; common difference of 30 K. Ordinate: maximum temperature difference (DTA) or maximum derivative of extinction difference (UV) sample/reference, referred to ceric salt concentration.

Therefore, it is better to divide the concentration effects contained in such a plot into two two-dimensional codes [13,15,17,21]. Table 2 gives examples of such codes, applied to the initial temperature, $T_0$, peak temperature, $T_m$, and end temperature, $T_e$, vs. the relative signal height, for the normal series (Ce + MA); a direct comparison with some two-reaction models, and with the hitherto best seven-step mechanism MAC7 (cf. Fig. 6) is presented.

Further conclusions may be obtained from the mechanistic diagrams of the systems (examples in Fig. 5). The evaluation strategy used was again the assumption of a one-peak signal where further overlapped peaks were seen as distortions [14,27]. Only in minor cases were separate evaluations of more isolated individual peaks tried (preferentially, $\alpha$-peaks).

For several totally evaluable series, the undirected concentration codes [17,22] of the mechanistic coordinates, $S$, $M$(init) and $M$(ov) are summarized in Table 3. The last columns contain the regions in the mechanistic overall diagram, respectively at the ends of the concentration or heating rate interval as well as in regions revealing both $S$ = const. and $M$ = const. (cf. Fig. 5). Some model codes were appended. Considerable difficulties appeared in the application of the one-step strategy to TA and GLY since often formally negative rate coefficients were obtained. This was due to either splitting into several peaks, or an excessive reaction rate at the lowest possible initial temperature [13] which required extrapolations to constant heating in the initial range. Therefore, the formal activation data, a prerequisite for the mechanistic interpretation, could not be calculated for some series of Table 1.

TABLE 2

Concentration codes of relative signal height and characteristic temperatures for series 1 and 1u of Table 1 [13,15]

| Technique/subject | $r_m/[Ce^{4+}]_0$ [a] | Temperatures at | | |
|---|---|---|---|---|
| | | Onset | Peak maximum | End |
| DTA experiments | − c + − c | c − c (+ c) [b] | (c) − c (+ c) | c − (c +) c |
| simulations | | | | |
| P1A:A → B(+A) → | + + + c c | c c − (c) + | c c − − c | c − c − (c) |
| P2A:2A → B(+A) → | + c + + + | − (c) − − (c) | − − − − − | − − − − − |
| G12:A ⇌ B+B | (c) − − − (c) | (c) − c + + | (c) − − − − | c − − − − |
| Model MAC7 (Fig. 6) [c] | c c − − (c) | (c) − (c − c) | (c) − c (+ c) | (c) c − (+) c |
| UV experiments | (c) − − (c) c | + c − + (c) | (c) − c − (c) | c c + − c |
| simulations | | | | |
| Model MAC7 | (+) − − c c | (c) − c − c | c (+) − − (c) | c + c − − |

+, increasing, −, decreasing, c, constant, parentheses, uncertain. One symbol represents a concentration range of nearly equal length, referred to the logarithmic concentration axis. Hence, repetition of symbols indicates the appearance of a longer period of retained feature.

[a] $r_m$ = maximum temperature difference sample/reference (DTA) or maximum rate of extinction change (UV).

[b] Extrapolations were necessary for high $Ce^{4+}$ concentrations because of too early start of reaction (near to the melting point!).

[c] cf. Table 6.

TABLE 3

Dynamic codes and particular regions in the "mechanistic diagram" [14]

| Acid | Series | Species varied | Shape index | Reaction type index | | Region [c] for | | Special situation | |
|---|---|---|---|---|---|---|---|---|---|
| | | | | Initial | Overall | low concentration | high concentration | Region | Conc. ($10^3$ M) |
| MA | 1 | Ce | (c)vc(v)c | (c)wwc | (v)cw(c) | C | I | (1) | 10 |
| | Mechanism | MAC 7 | (c)v(c)v(c) | cwcvc | cwc(w) | C | ØE | (1) | 10 |
| | Mechanism | P2A | Cwc [a] or cwwc [b] | cwwc | cw(wc) | Ø | C | – | – |
| | 1u | Ce | (cv)wcv(c) or w(w)cv(c) | (vc)cwc | c(v)c(w)c(w) | DF | AC | A/(2) | 0.22 |
| | Mechanism | MAC7 | cwc(vc) | (v)cv(w) | (v)cvw(w) | C | AC | ØC | 0.22 |
| | 1i | MA | wwwc | (w)vc(v) | (c)cwc(v) | C | C | (1) | 0.25 |
| | 1ui | MA | vcw | c(w)w | cwcv | B | GH | AC | 0.25 |
| TA | 2 | Ce | cvc(w) | cw(wwc) | (c)ww(c) | F | (2) | A | 120 |
| | 2α | Ce | cvc(w) | ww | (c)ww(c) | D | BF | – | – |
| | 2u | Ce | (c)wwww | cwwww | c(w)wc(w) | AC/(1) | C | – | – |
| | 2uα | Ce | v(c)v or wvcv | wwcv | cvcv | F | F/AF | I | 4 |
| GLY | 3α | Ce | (v)cw(w) | wc(v) | (c)ww(w) | G | G | GH | 10 |
| | 3u | Ce | wwwwcw | w(c)ww | cwcw | BF | A | EH | 0.1 |
| | 3iu | GLY | vcv(c)wcwc | cvcwwv | cv(c)ww | Ø | C | C | 2 |

c = constant; v = variable (monotonous); w = variable (includes extremum value); parentheses = questionable. Sequence in the order of increasing starting concentration. In contrast to the codes in Table 2, the length of the concentration interval is not included in the code; i.e., repetitions of neighboured symbols do not occur, when "w" is excepted (ww = one maximum, followed by a minimum, or vice versa). These dynamic codes represent a phenomenological characterization of any reaction based on the law of mass action [13,14,17,22].

[a] $E_2 < E_1$. [b] $E_2 > E_1$. [c] cf. Tables 4 and 5.

For malonic acid, the ranges used for the concentration of both components and the final reaction types are presented in a two-dimensional form in Table 4, whereas the results of the variation of the heating rate are summarized for all acids in Table 5.

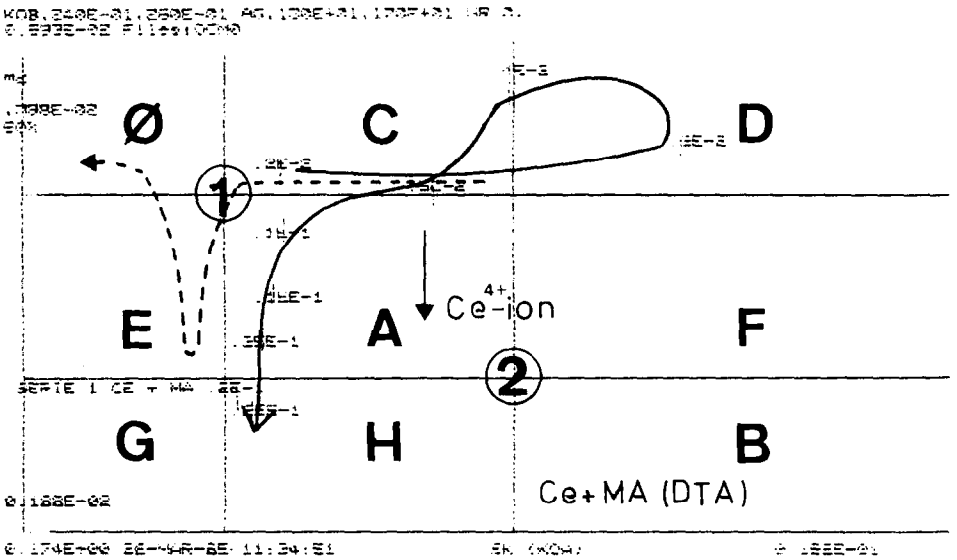


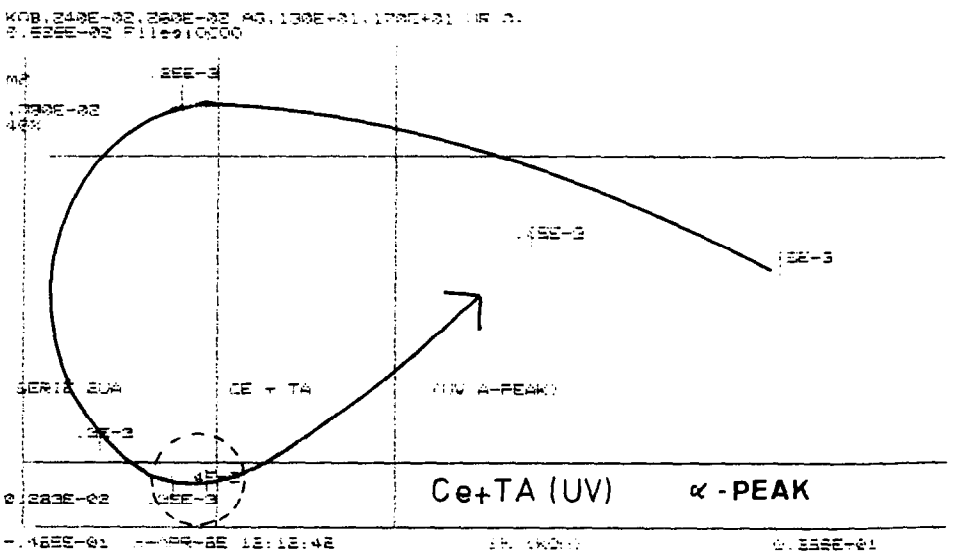

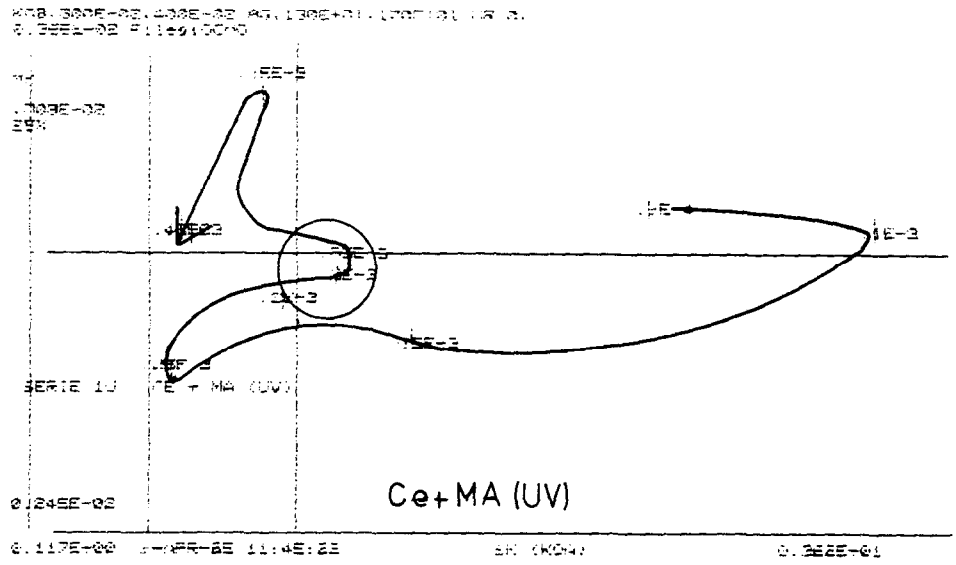


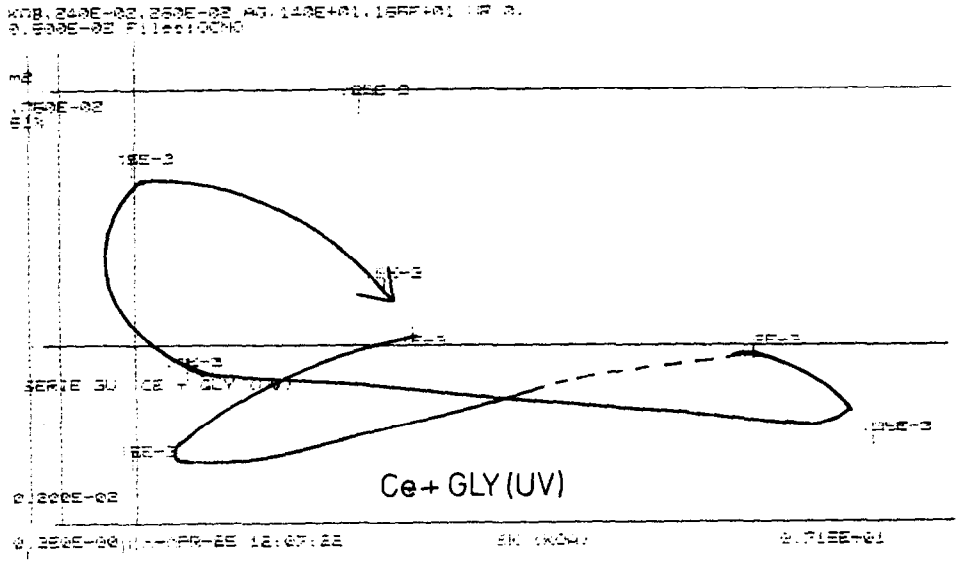


Fig. 5. Mechanistic overall diagrams for four normal series. Computer forms. Numbers: initial concentrations of ceric sulphate for the cross-marked individual experiments. Letters: mechanistic regions [18]. Thin axis system: represents the cases $S = S_1$ and $S_2$, $M = M_2$ and $M_1$. Thick curves: assumed mechanistic paths for increasing starting concentration (numbers) from the experiments. Dotted curve: same, but from simulations based on scheme MAC7.

## DISCUSSION

### *General*

A comparison of our results, obtained at temperatures from 265 K up to 370 K, with results of isothermal studies from the literature, usually per-

TABLE 4

Influence of both reactant concentrations on overall reaction type and activation parameters for the system ceric sulphate/malonic acid

| MA (M) | Ceric sulphate (M) | | | | |
|---|---|---|---|---|---|
| | $10^{-5}$ | $10^{-4}$ | $10^{-3}$ | $10^{-2}$ | $10^{-1}$ |
| $10^{-5}$ | | cf. ref. 11 | | | |
| $10^{-4}$ | | $^{75}$F | AF[35] | (2)[83]A | DTA method |
| $10^{-3}$ | | [83]BF | | C | |
| | | 0 | | | |
| | | E[88] | C/(1)[42]AC[30] | (1)[33] AG[62] | |
| $10^{-2}$ | | I | | | |
| | | EH[66] | | A[58] | cf. refs. 9 and 10 |
| $10^{-1}$ | | | | (2)[30] | |
| | | | | C[33] | |
| $10^{0}$ | UV method | | | | |

Reaction types: Based on two-reaction models in the mechanistic diagram; cf. ref. 14. Rough classification:
(1) = unimolecular or pseudounimolecular process.
(2) = bimolecular process; reactant ratio 1:1.
A = general bimolecular process, or concurrent reactions with primarily dominating bimolecular process, or consecutive processes, or opposing reaction of second order.
C = autocatalytic process or concurrent reactions of first order i presumably concurrent reactions of different order or consecutive reactions with unimolecular initiating process.
E = recoupling or autocatalytic consecutive processes or consecutive processes with termination of zeroth order (unusual type).
F = more complicated; perhaps consecutive reactions of second order and low $A$ factor of the second process.
G = consecutive processes of mixed order or more complicated.
Double letters: near the limits of the respective regions.
Numbers: overall activation energies in kJ $mol^{-1}$ according to the regions.
The line separates the range of the DTA experiments from that of the UV experiments. The working ranges due to the references cited are also indicated. Regions 0, B, H see Table 5.

formed near room temperature, leads to some problems. Nevertheless, we were able to confirm many results, especially heats and activation parameters if the concentrations of the reactants were comparable. Moreover, since our experimental concept covers a much wider range of conditions, extrapolations from our results to unexplored condition ranges could be attractive. This is a consequence of the universal estimation of various reaction-related parameters by providing for an adequate series of experiments.

The partially complicated dependence of the overall enthalpy upon the concentration of the varied reactant (cf. Table 1) needs more detailed discussion; but surely other codes offer better access to the kinetics [14]. The complexity indicates that the reaction between ceric ion and malonic acid is,

TABLE 5

Ranges of constant parameters, reaction types and gross activation energies ($E$) in heating rate series

| Acid | Series | Number of c-periods | | | | | | Heating rate (K min$^{-1}$) | | | | | | | | | | | |
|---|---|---|---|---|---|---|---|---|---|---|---|---|---|---|---|---|---|---|---|
| | | $T_0$ | $v_{rel}$ | $S$ | $M_0$ | $M$ | | 0.1 | 0.2 | 0.3 | 0.5 | 1 | 1.5 | 2 | | 3 | | 5 |
| MA | 1h | 1–2 | 1–2 | 2–3 | 1–2 | 2 | init. | B/(2) | | DF | AD | | (1) | AG | A | | | (1) |
| | | | | | | | E | | | | | | | | | | 78 | |
| | | | | | | | | | | | | ... | 50 | | | | ... | |
| | | | | | | | ov. | B/(2) | | BF | C | AH | | EG | | | | = (1) = |
| | 1hu | 1? | 1–2 | 2 | 2 | 2 | init. | | | AG | E | A | GE | (1) | E | | | G((1))AC |
| | | | | | | | E | | | ... | 75 | | 50 | ... | | ... | | ..... |
| | | | | | | | ov. | | | (2) | AH | G | = EG = | ~ (1) | | | | A |
| TA | 2hu | 0 | 1–2 | 1 | 2–3 | 1–2 | init. | | | C | | H | (1) | CD | | | | DF |
| | | | | | | | E | | | ... | ... | 62 | ... | ... | | | | 74 |
| | | | | | | | ov. | | | C | A | (1) | OC | C | | CD | | D |
| GLY | 3hu | 1–2 | 1–2 | 2 | 3 | 2–3 | init. M | | | | C | AC | = (1) = | GH | | BH(2)H | | G H |
| | | | | | | | E | | | ... | ... | | ...80 | | | ...77... | | |
| | | | | | | | ov. M | | | | C | D? | (1)AG | H | | C | A | (2) |

Symbols: see Table 4, cf. ref. 14.

B = consecutive reactions of second order (including cross terms!), reactions of third order, etc. D = unusual types; complicated and not yet explored. 0 = reaction of zeroth order, heterogeneous reactions. H = consecutive processes of second or higher order, second-order opposing reactions. Numbers: overall activation energies in kJ mol$^{-1}$.

(———) $M$-index constant; (· · · · · ·) $S$-index constant; ( = ) $M$ and $S$ constant.

in general, not a simple bimolecular process [23]. Though, in contrast to the experiments with TA and GLY, only one peak is observed, our results give indications to two or more processes which govern the overall kinetics in certain concentration ranges, where realistic activation energies can also be presented.

*Temperature–height diagram [15]*

Especially in the DTA measurements and for increasing $Ce^{4+}$ concentration (normal series), a first-order point is approached for MA (apart from an intermediate point), TA and GLY; it appears as a final, converging point, but below it will be shown that there is no true unimolecular reaction under these conditions (Fig. 4, Table 4). On the other hand, in the first part of the inverse MA series (1i) there is a vertical straight line rather than a point when the MA concentration is increased (codes: ccc + + for initial temperature, and − c − − 0, i.e., final approach to zero, for the relative signal height). Usually, this should indicate a dominating bimolecular process for insufficient MA concentration [15]. However, anomalies are the partially positive concentration shifts of the initial temperature (cf. series 1 in Table 2, and series 1u with code + c − + (c + )c) which characterize the starting processes. Within the simple two-reaction models, such a shift is only compatible with the mechanism P1A (first-order starting process, and reaction of the formed product with educt) or G12 (opposing processes with first-order forward reaction and bimolecular reverse reaction).

In the normal UV series with MA, there are only poor indications for a first elementary concentration range near the minimum concentration, ca. 0.0002 M $Ce(SO_4)_2$, indicating first order (point; corresponding activation energy $E = 75$ kJ mol$^{-1}$), and perhaps a second at slightly raised concentration (0.003 M), indicating second order (horizontal straight line; $E = 35$ kJ mol$^{-1}$; cf. Table 5); however, the total changes of $T_0$ and $\theta_m/[Ce^{4+}]_0$ are relatively small.

For GLY, the UV temperature/height studies exclude that for increased ceric content a bimolecular process is rate-determining; a decreasing signal height, but a later inconsistent increase of the initial temperature are obtained: a distinct indication for inhibition effects or reverse reactions. In the corresponding DTA plot of Fig. 4, involving higher concentrations of reactant, this late temperature increase is less pronounced.

Further indications for the type of mechanism are given by pattern recognition, using the mechanistic coordinates [14,18,21].

*Mechanistic diagram*

The undirected mechanistic codes were introduced and calculated for all two-reaction models in order to reach a general characterization of a

mechanism, mainly independent of the activation parameters of the steps [17]. The position of an experimental point of a complex process in the mechanistic diagram depends not only on the type of mechanism, but also on the conditions with respect to the activation parameters concerned [27]. The "dynamic" mechanistic codes, however, which consider the dependence of such a point on a starting concentration or the heating rate, neglect both the position and the direction of change; both increase or decrease of a quantity means, then, "variable". Our computer simulations have shown that signal curves based on different activation data yield the same mechanistic codes if they are derived from the same mechanism. Only in special cases, e.g., for opposing reactions, are there several codes for one mechanism depending on whether the difference of certain activation energies is positive, zero or negative [17]. Table 3 shows such codes for the experiments with MA, TA and GLY and two simulated model series. The resulting sigmoid plots (w-periods) are characteristic of recoupling, i.e., occurrence of both consecutive and concurrent reactions, whereas coincident c-periods with constant $S$ and at least one constant $M$ ($M$(init) or $M$(ov)) indicate a concentration range where the reaction proceeds elementarily or pseudo-elementarily. There is a partially satisfactory agreement of the experimental codes of the Ce/MA system with the codes of the model mechanism MAC7, especially for the DTA experiments, where the error limits are lower than for the UV experiments.

The mechanistic curves of the concentration dependence, as kinetic fingerprints of the systems, are presented for some series in Fig. 5 (cf. Fig. 4, Tables 3, 4 and 5), and are now discussed in detail.

*Malonic acid*

In the UV measurements and for medium concentrations of ceric sulphate (0.0002 M), a stationary range with $S = S_2$, but $M = M_1$ prevails (type II), whereas for maximum concentration a true first-order range is observed.

In the DTA experiments, there is a rather first-order situation for low $Ce^{4+}$ concentration, exhibiting a distinct tendency to a parallel first-order process or even to an autocatalytic process (region C). Increasing concentration primarily leads to the boundary between regions A and C or F, which is rather typical of consecutive reactions with an initiating first-order reaction. Subsequently, for 0.015 M $Ce(SO_4)_2$, the first-order range is passed intermediately. For high ceric ion concentrations and in contrast to the UV measurements, the approach of the overall $S/M$ point to the regions A/G (Table 3 [18]) signals the type I ($S = S_1$; $M = M_2$) which excludes a pseudo-unimolecular process.

Thus, the DTA studies reveal two periods of apparently elementary and a further period of pseudo-elementary behaviour. The second and third periods were confirmed by stationary points in the respective temperature–height plot. The corresponding activation energies are 42, 33 and 62 kJ $mol^{-1}$

(Table 4); the value cited by Barkin et al. [10] (48 kJ $mol^{-1}$; spectroscopic and titrimetric measurements) is only obtained for a low concentration of ceric sulphate, as also in the UV experiments, whilst the value of Sengupta and Aditya [11] (62 kJ $mol^{-1}$) is observed for low $Ce^{4+}$, but higher MA concentrations.

The inverse DTA series (1i) revealed that the second-order range is passed for MA excess (Table 4).

In the UV studies, only the third stationary period of the temperature–height diagram (horizontal line) was identified in the mechanistic diagram (type II; $S = S_2$; $M = M_1$). This indicates consecutive bimolecular processes, perhaps catalytic in nature. The DTA- and UV-generated mechanistic curves in Fig. 5 represent different active subunits of the same basic mechanism. Obvious differences are caused by the very different concentration ranges for both techniques (cf. Table 4). Further, this diversity is strengthened by the fact that processes stemming from organic radicals and oxygen may partially and irreversibly lead to stable products, but without participation of ceric ion; such final steps are not indicated by the absorbance measurements and do not influence the previous kinetics.

*Tartronic acid*

The overall evaluation of the normal UV series revealed a movement of the mechanistic $S/M$(ov) point from the A/H boundary to the C/D boundary, indicating a transfer from a very complicated, unexplored type to a rather autocatalytic type of process. According to a preliminary UV study of the $\alpha$-peak, the couple of initiating reactions corresponds to a nearly cyclic mechanistic curve, starting from the unusual D zone (or B zone for the $M$(init) value; cf. Table 5), and passing through regions C, 0, E, I and A until the D region (or B region) is reached again. Complementary results, but without such a cyclic movement, were observed in the inverse UV series (2iu).

From the separate UV $\alpha$-peak, we estimated a stationary range near the I-zone for $Ce^{4+} = 0.00003$ M, with an activation energy of 120 kJ $mol^{-1}$ and log $A = 28.2$; these unrealistically high activation parameters confirm that an elementary process cannot be found even by the use of a peak-splitting procedure.

An analogous analysis of the $\alpha$-peak of the DTA curve with 0.03, 0.06, 0.081 and 0.12 M ceric sulphate suggested validity of the D region for the lowest, but of the B/F border region for the highest ceric ion concentration (consecutive or opposing reactions of higher order or type P2A).

*Glyoxylic acid*

The normal UV series of GLY is characterized by peak-splitting (cf. Fig. 2). The overall mechanistic curve shows a cyclic course, beginning at the B/F border, then continuing inside the B-region (consecutive reactions of

higher order), and approaching the second-order source point (2) twice, namely for low and medium ceric ion starting concentrations (Fig. 5). On further increase of ceric sulphate, the boundary of regions A and F is passed precisely when the temperature/height plot nearly follows a horizontal straight line from right to left (opposing second-order steps, cf. ref. 15 and Table 2; recombination of two C-fragments?).

*Monobromomalonic acid*

The DTA experiments with BMA (involving five different concentrations of ceric ion) revealed a trend from a preferentially autocatalytic range (boundary 0/C) to the "pseudo-elementary" point I, which analogously appeared in the system Ce/MA.

*Heating rate*

For MA, a change of the heating rate, $m$, gives no direct indications for peak-splitting. However, there is a continuous change of the mechanistic regions concerned in both the DTA and UV studies, and there are ranges of $m$ where the signals exhibit nearly first- or second-order character (Table 5). In the range somewhat below our standard heating rate ($m = 1.5$ K min$^{-1}$), we observe a nearly first-order process for the specified concentrations, showing the mentioned activation energy of ca. 48 kJ mol$^{-1}$.

The UV experiments with TA reveal several peaks and a pertinent change of the region with increased heating rate (C → A → (1) → D) in the overall diagram, but no distinct tendency for merging or additional splitting of peaks. Whilst in the normal concentration series with TA only unrealistic activation energies could be calculated, the normal UV heating rate series yields two lower, rather probable values, namely 62 kJ mol$^{-1}$ for low and 74 kJ mol$^{-1}$ for high heating rates (see Table 5). A simplification of the mechanism to rate-determining steps is only recognized in the first range.

In contrast, the UV signals of the Ce/GLY system become simpler if $m$ is increased; the peaks are then merging. The $S/M$(ov) curve reveals a trend from region C passing the first-order range ($E = 80$ kJ mol$^{-1}$) and the rather unspecific region A, ending at the second-order source point.

*Reaction heats*

DTA experiments open a further path, the energetic approach to the problems. The overall enthalpy for the MA reaction studied by Körös et al. by isothermal calorimetry, is 535 kJ mol$^{-1}$ MA for six-electron change (2–10-fold excess of ceric salt) [23]. In our inverse DTA series of this system (1i in Table 1), the enthalpy increased to even 2570 kJ mol$^{-1}$ MA for the minimum feed of 0.002 M MA (10-fold excess of $Ce(SO_4)_2$), which indicates a strong interference of oxidation processes, possibly chain reactions.

If we use the gas-phase enthalpy increments of Franklin [26], the thermochemical equations of the primary steps are

$$Ce^{4+} + \underset{(MA)}{CH_2(COOH)_2} = Ce^{3+} + \cdot CH(COOH)_2 + H^+ - (426 - X)\ \text{kJ mol}^{-1} \quad (1a)$$

$$Ce^{4+} + \underset{(TA)}{CHOH(COOH)_2} = Ce^{3+} + \cdot COH(COOH)_2 + H^+ - (426 - X)\ \text{kJ mol}^{-1} \quad (2a)$$

$$Ce^{4+} + \underset{(GLY)}{CHO{-}COOH} = Ce^{3+} + \cdot COCOOH + H^+ - (331 - X)\ \text{kJ mol}^{-1} \quad (3a)$$

$X$ represents the ionisation energy in the solution; since $X$ is in the region of $+110$ kJ mol$^{-1}$ [27–29], steps 1a–3a are endothermic. However, the radicals thus formed must vanish rapidly by the exothermic disproportionation reactions:

$$2\cdot CH(COOH)_2 + H_2O = \underset{(MA)}{CH_2(COOH)_2} + \underset{(TA)}{CHOH(COOH)_2} + 686\ \text{kJ mol}^{-1} \quad (1b)$$

$$2\cdot COH(COOH)_2 = \underset{(TA)}{CHOH(COOH)_2} + \underset{(GLY)}{CHO{-}COOH} + CO_2 + 910\ \text{kJ mol}^{-1} \quad (2b)$$

$$2\cdot CO{-}COOH + H_2O = \underset{(GLY)}{CHO{-}COOH} + HCOOH + CO_2 + 778\ \text{kJ mol}^{-1} \quad (3b)$$

where all stable compounds were isolated as reaction products [5,10]. Hence, only half of the acid molecules are consumed in the steps a/b. Neglecting all other interactions, one obtains the following stoichiometric equation for the system Ce/MA:

$$6Ce^{4+} + CH_2(COOH)_2 + 2H_2O = 6Ce^{3+} + HCOOH + 2CO_2 + 6H^+ + 1.75(197 + X)\ \text{kJ mol}^{-1} \quad (4)$$

Using the heat of ref. 23, this corresponds to an $X$ value of 108 kJ mol$^{-1}$ if formic acid and carbon dioxide are the only reaction products.

These heats are dramatically surpassed in many experiments, especially for small inputs of ceric sulphate (Table 1), which signals that, in contrast to eqn. (4), one molecule of ceric salt may induce the oxidation of several MA, TA and/or GLY molecules, necessarily under the participation of molecular oxygen [10] (cf. legend to Fig. 6).

*General scheme and simulations*

Due to assumptions discussed in the literature, the complicated stoichiometry and kinetics should be caused by repeated redox reactions of ceric ion with various intermediates originating from the malonic acid molecule, such as TA, GLY and related radicals, $\cdot CH(COOH)_2$ (malonyl radical), $\cdot C(OH)(COOH)_2$ (hydroxymalonyl radical) and $\cdot CHO$ (formyl radical), before the stable final products, HCOOH, $CO_2$ and CO are formed [11].

The conditions are further complicated by an assumed rapidly reached equilibrium between the starting reactants, leading to a Michaelis–Menten-type behaviour in the first period of the reaction [11].

Under the non-isothermal conditions used here, we have only weak indications for such an equilibrium. However, we have unambiguous evidence that indeed repetitive concurrent/consecutive steps with ceric sulphate are involved. Pattern recognition reveals both for the temperature/ signal height diagrams [15] (Fig. 4 and Table 2, series 1 and 1u) and for the mechanistic diagrams (Fig. 5, Tables 3 and 4) [14] that the respective two-reaction model P2A ($A + B \rightarrow C$; $A + C \rightarrow$ prod.) has to be discussed as a skeleton mechanism at slightly increased concentrations of ceric salt, even in the UV experiments focussed on the respective reactions. Our preliminary working model should satisfy the following conditions:

(1) for MA as a substrate, a minimum of two steps which appear as rate-determining under non-isothermal conditions (cf. Tables 4 and 5) are required;

(2) subsequent to a pre-equilibrium, one initiating step is the normal bimolecular reaction between $Ce(SO_4)_2$ and MA which is preferred at low concentrations of ceric ion;

(3) ceric ion undergoes additional, faster reactions with the transients TA and GLY;

(4) the activation data and heats of these reactions have to be compatible with the data of the signals obtained using the systems Ce + TA and Ce + GLY;

(5) in order to explain the oxygen effects, the generation of organic radicals and their consumption has to be considered.

Combining both the results of other groups with the MA system and our own experiences with 23 different mechanisms, we selected the following nine-step mechanism as a working model:

$$CE + MA = CEK \qquad (R1)$$

$$CEK + CE = 2CER + MA \qquad (R2)$$

$$CEK + MA = CER + MOH + 1/2MA + 1/2TA \qquad (R3)$$

$$CEK + MOH = CER + 1/2MA + 1/2TA + GLY \qquad (R4)$$

$$MOH = GLY \qquad (R5)$$

$$CE + TA = CER + 1/2TA + 1/2GLY \quad (R6)$$

$$CE + GLY = CER + 1/2GLY + FOR \quad (R7)$$

$$CEK = CE + MA \quad (R8)$$

$$CEK = CE + 1/2MA + 1/2TA \quad (R9)$$

The species are: $CE = Ce(SO_4)_2$; $FOR = HCOOH$; $CER = Ce_2(SO_4)_3$; $CEK$ = complex $Ce(SO_4)_2 \cdot \cdot$ MA; MOH = unstable peroxide $MA \cdot O_2$. $H^+$ was neglected because it was taken as constant; substances irreversibly leaving the system, such as $CO_2$, $Br_2$, and end products without kinetic effect were also neglected.

This model includes reversible complex formation solely between ceric ion and MA; also the expected oxygen effects were considered only for MA; the idea was to start with a simple model, which at a later stage could be expanded. It is based on the known rate constants accessible from the cited references [2]. Since activation data were only available for the reaction 1 in Fig. 6, we have used fitted activation energies for signal modifying steps and roughly estimated values for the other, redundant steps, calculated from the rate constants and from realistic $A$ factors due to the type of the process.

For the fast reactions 2a, 3a, 4a, R8 and R9, the knowledge of the (probably small) values of the activation energies is surely less important than that of the ratios of the rate coefficients, compared to reaction 1a. Further, for the opposing steps R1 and R8, primarily the difference of the activation energies is of interest, because of determining whether the equilibration process is exothermic or endothermic. We have assumed a relatively small difference of $E_8 - E_1 = 1.8$ kJ mol$^{-1}$, corresponding to a weakly exothermic process.

Hitherto, we have tested this model by files of 15 various DTA experiments and 10 UV experiments with different initial concentrations of ceric sulphate and MA. Reactions R6 and R7 were "calibrated" by the initial activation data of the TA and GLY experiments. Because of missing information on the temperature dependence of steps R1 and R8, it is difficult to study the influence of this pre-equilibrium on the prevailing $A$ factors of reactions R6 and R7. Further, the general results with the nine-step model were not very satisfactory; therefore, it was proven to be more effective to consider first a simplified version (MAC7) which does not assume a complex between Ce and MA (Fig. 6). Table 6 presents the results of a comparison of this model with 11 arbitrary DTA experiments, indicating that the adapted frequency factors of steps 3 and 5 in Fig. 6 show variations up to 1:10, the enthalpies of step 5 up to 1:2, whereas the variances of all other parameters are much smaller. The UV signals studied obey roughly the same model using the signal parameters (here: differences of extinction coefficients at 317 nm) of about 10000 for all steps without step 5 (which then has the signal parameter zero). This means that the model seems to be a satisfactory starting basis, since bad reproducibility of even

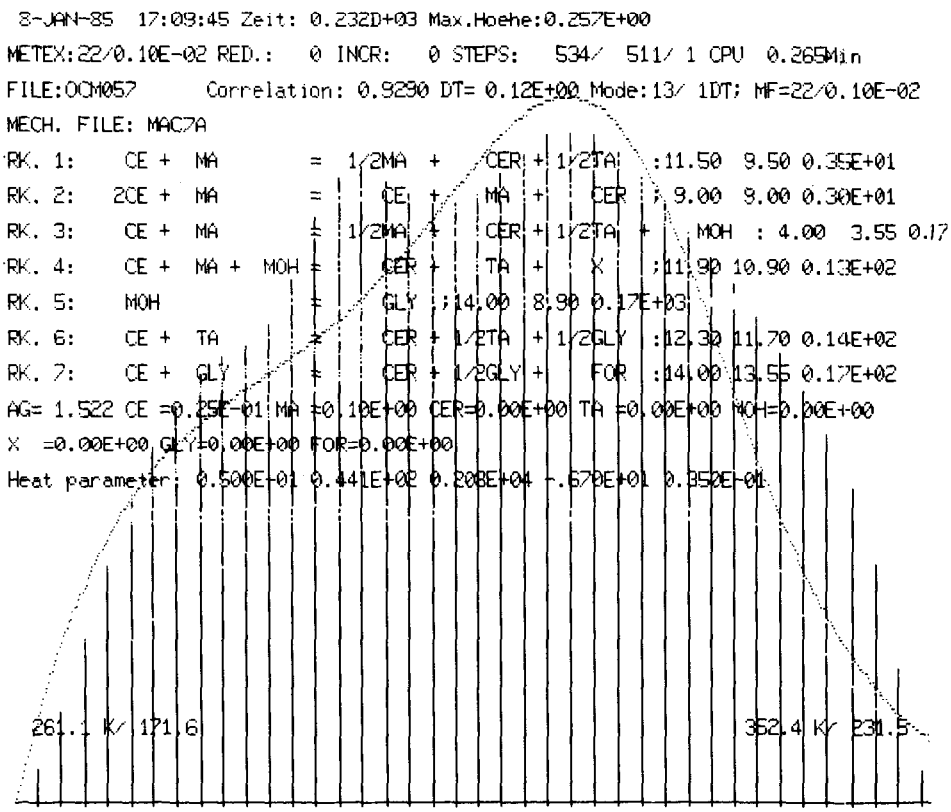


Fig. 6. Test of theoretical reproduction of a special DTA curve with MA. Computer form (program METEX [17]). Mechanism used: MAC7. Characteristic data for the steps: activation energy—log($A$ factor)—reaction enthalpy. Dimensions: kcal, min, mol. Initial concentrations: $Ce(SO_4)_2$, 0.025 M; MA, 0.1 M. Heating rate: 1.5 K $min^{-1}$. Remarks to special steps: Reaction 1: combination of reactions 1a and 1b (see text). Reaction 2: deactivation step explaining phenomena at small Ce concentrations. Reaction 3: combination of eqns. 1a, 1b and addition of molecular oxygen to the intermediate malonyl radical. Reaction 4: combination of reactions 1a, 1b with peroxide decomposition resulting in reformation of oxygen. Reaction 5: unimolecular decomposition of the peroxide (decarboxylation?). Reaction 6: combination of text reactions 2a and 2b. Reaction 7: combination of text reactions 3a and 3b.

steps 3 and 5, which describe the distortions by access of oxygen, had been expected. Indeed, there were no indications for a late peak according to reaction 5 if the MA reaction was studied under argon gas (cf. Fig. 1A).

Theoretical DTA curves calculated from the model MAC7 reveal similar concentration codes as those obtained from our experiments (Tables 2 and 3). However, Fig. 5 shows that only a part of the mechanistic line derived from the experiments is reproduced by the respective theoretical curve. This may indicate that the mechanism MAC7 is at least incomplete, if not wrong; on the other hand, the mechanistic coordinates are often extremely depen-

TABLE 6

Reproduction of experimental DTA curves by mechanism MAC7 (cf. Fig. 6)

| Exp. File OCM0 | Concentrations | | Fitted parameters | | | | | Correlation coefficient |
|---|---|---|---|---|---|---|---|---|
| | Ce | MA | $F1$ | $F3$ | $F4$ | $F5$ | $S5$ | |
| 392 | 0.002 | 0.025 | 9.60 | 5.54 | 11.4 | 9.00 | 100 | 0.9647 |
| 382 | 0.003 | | 9.60 | 5.55 | 11.3 | 8.90 | 100 | 0.9514 |
| 402 | 0.010 | | 9.70 | 4.25 | 11.5 | 10.20 | 150 | 0.8070 |
| 412 | 0.015 | | 9.60 | 4.42 | 11.5 | 9.80 | 80 | 0.9428 |
| 052 | 0.025 | 0.005 | 9.70 | 5.75 | 11.2 | 9.30 | 150 | 0.9278 |
| 056 | | 0.015 | 9.40 | 4.50 | 11.1 | 9.20 | 80 | 0.8525 |
| 003 | | 0.025 | 9.70 | 4.80 | 11.3 | 9.90 | 80 | 0.9552 |
| 023 | | | 9.70 | 5.45 | 10.8 | 8.95 | 120 | 0.8785 |
| 057 | | 0.100 | 9.50 | 3.55 | 10.9 | 8.90 | 170 | 0.9290 |
| 058 | | 0.200 | 9.45 | 3.46 | 11.1 | 8.90 | 150 | 0.8138 |
| 352 | 0.035 | 0.025 | 9.42 | 4.54 | 11.8 | 9.55 | 80 | 0.9545 |
| Average | | | 9.61 | 4.72 | 11.35 | 9.28 | 112 | 0.9055 |
| Standard deviation | | | 0.18 | 0.78 | 0.41 | 0.47 | 34 | 0.0571 |

Heating rate: 1.5 K $min^{-1}$ + 0.12.
Dimensions: min, kcal, l $mol^{-1}$.
Parameters: $F1$ = log ($A$ factor) of reaction 1; $S5$ = signal parameter (here: neg. reaction enthalpy) of reaction 5.
Other data used: $F2 = 9.20$; $S1 = 2.4$; $S2 = 3$; $S3 = 17$; $S4 = 12$.
Activation energies: $E1 = 11.5$; $E2 = 9.0$; $E3 = 4$; $E4 = 11.9$; $E5 = 14.0$.
Reactions 6 and 7: see Fig. 6.

dent on the difference of the activation energies of special steps involved [27], even for consecutive steps. Therefore, the dynamic codes are a better criterion for a first comparison, aimed at identification of a model in principle.

The activation energies of the parallel steps 1–4 and, therefore, also the respective $A$ factors cannot be accurately determined from single experiments; an approximate calculation leads to the following ratios of the rate coefficients at 298 K: 1 : 2.8 : 0.5 : 2.9.

## CONCLUSION AND OUTLOOK

Knowledge of the formal kinetics is a prerequisite for drawing conclusions on the structural, microscopic advancement of a reaction.

Although we are not convinced of having already found the best reaction mechanism for the title systems, our concerted studies indicate the further path to be followed. For very complex signals, our unpromising experiences with their tedious theoretical re-simulation from models may suggest that application of this strategy alone is inappropriate for finding adequate

reaction mechanisms. Preference should first be given to the other paths described. Obviously, these more systematic ways, based on the most appropriate of more than 30 readily available parameters, must finally lead to the best mechanism for a given accuracy requirement. The concentration codes, meanwhile developed for all basic two-reaction models [17], and the heating rate codes were introduced for delegating the outlined strategies to the computer. By an automatic discussion of recorded experimental series, the chemist could be liberated from the tedious job of model searching in order to construct a microscopic model which is compatible with thermodynamic and structural requirements.

It will be important to study not just the position of one experiment in a "mechanistic map", but also the type of change of this position with respect to appropriate condition parameters (dynamic codes [22,30]). Therefore, computer simulations will be necessary to a larger extent, but in a more systematic way than directly trying to reproduce various experimental signals [31]. We have to learn what changes of the dynamic codes will appear in general if an additional reaction step is appended to a prevailing reaction mechanism. This seems to be the only realistic way to reveal more and more complicated mechanisms systematically, and to reach an increasingly better approach to the reality.

The third alternative, precalculating mechanistic patterns for all imaginable three-reaction models, four-reaction models, etc., has no real chance of successful application to very complex processes, such as occur in the title systems; this strategy must decay in the unlimited variety of combinatorial possibilities.

## ACKNOWLEDGEMENTS

Mrs. G. Mummerz, Mrs. B. Pirke and Mr. E. Theisen performed the partially difficult measurements and assisted me in data processing. I am grateful to these co-workers and to Mr. H.-D. Schmitz of the Joint Computer Department of the Max-Planck Institutes for Coal Research and Radiation Chemistry.

## REFERENCES

1 R.J. Field, E. Körös and R.M. Noyes, J. Am. Chem. Soc., 94 (1972) 8649.
2 D. Edelson, R.M. Noyes and R.J. Field, Int. J. Chem. Kinet., 11 (1979) 155.
3 R.J. Field and R.M. Noyes, J. Chem. Phys., 60 (1974) 1877.
4 E. Koch and B. Stilkerieg, Thermochim. Acta, 29 (1979) 205.
5 J.J. Jwo and R.M. Noyes, J. Am. Chem. Soc., 97 (5422) 1975.
6 Z. Noszticzius, H. Farkas and Z.A. Schelly, J. Chem. Phys., 80 (1984) 6062.
7 R. Noyes, J. Chem. Phys., 80 (1984) 6071.

8 E. Körös, M. Varga and L. Györgyi, J. Chem. Phys., 88 (1984) 4116.
9 S. Barkin, M. Bixon, R.M. Noyes and K. Bar-Eli, Int. J. Chem. Kinet., 9 (1977) 841.
10 S. Barkin, M. Bixon, R.M. Noyes and K. Bar-Eli, Int. J. Chem. Kinet., 10 (1978) 619.
11 K.K. Sengupta and S. Aditya, Z. Phys. Chem., Neue Folge, 38 (1963) 25.
12 E. Koch and B. Stilkerieg, in W. Hemminger (Ed.), Thermal Analysis, Vol. 1, Proc. 6th Int. Conf., Bayreuth, Birkhäuser, Basel, 1980, p. 75.
13 E. Körös and E. Koch, Thermochim. Acta, 71 (1983) 287.
14 E. Koch, Thermochim. Acta, 56 (1982) 1.
15 E. Koch, Thermochim. Acta, 76 (1984) 105.
16 E. Koch and B. Stilkerieg, in E. Marti, H.R. Oswald and H.G. Wiedemann (Eds.), Angewandte chemische Thermodynamik und Thermoanalytik, Birkhäuser, Basel, 1979, pp. 210–215.
17 E. Koch, in B. Miller (Ed.), Thermal Analysis, Vol. 1, Proc. 7th Int. Conf., Kingston, Ont., 1982, Wiley, Chichester, 1982, pp. 71–79.
18 E. Koch, Angew. Chem., 95 (1983) 185; Angew. Chem. Int. Ed. Engl., 22 (1983) 225.
19 E. Koch, Chem. -Ing. -Tech., 37 (1965) 1004.
20 E. Koch, B. Stilkerieg and L. Carlsen, Ber. Bunsenges. Phys. Chem., 83 (1979) 1238.
21 E. Koch, Thermochim. Acta, 82 (1984) 293.
22 E. Koch, Thermochim. Acta, 49 (1981) 25.
23 E. Körös, M. Orban and Zs. Nagy, Acta Chem. Acad. Sci. Hung., Tomus, 100 (1979) 449.
24 E. Koch and B. Stilkerieg, Thermochim. Acta, 27 (1978) 69.
25 E. Koch and B. Stilkerieg, J. Therm. Anal., 17 (1979) 395.
26 See, e.g., d'Ans-Lax, Taschenbuch für Chemiker und Physiker, Vol. II, Organische Verbindungen, 3 Aufl., Springer, Berlin, 1964, p. 1047.
27 E. Koch, Angew. Chem., 5 (1973) 381; Angew. Chem. Int. Ed. Engl., 12 (1973) 381.
28 E. Koch, Tetrahedron, 26 (1970) 3503.
29 E. Koch, J. Therm. Anal., 6 (1974) 483.
30 E. Koch, Non-isothermal Reaction Analysis, Monograph, Academic Press, London, 1977, pp. 280–292, 362–375.
31 E. Koch, in K.H. Ebert, P. Deuflhard and W. Jäger (Eds.), Modelling of Chemical Reaction Systems, Springer, Berlin, 1981, pp. 216–225.